

**International Journal of Electric and Hybrid Vehicles**

ISSN online: 1751-4096 - ISSN print: 1751-4088

<https://www.inderscience.com/ijehv>

---

**Modelling and analysis of electric two-wheeler with novel planetary gear box transmission**

Aditya Paranjape, Amey Kulkarni, Mihir Kulkarni, Neeraj Kumbhojkar

**DOI:** [10.1504/IJFHV.2023.10054138](https://doi.org/10.1504/IJFHV.2023.10054138)

**Article History:**

Received:	07 June 2021
Accepted:	16 July 2021
Published online:	17 February 2023

---

## Modelling and analysis of electric two-wheeler with novel planetary gear box transmission

---

Aditya Paranjape\*, Amey Kulkarni,  
Mihir Kulkarni and Neeraj Kumbhojkar

Department of Mechanical Engineering,  
Vishwakarma Institute of Technology,  
Pune, Upper Indiranagar, India  
Email: aditya.paranjape17@vit.edu  
Email: amey.kulkarni17@vit.edu  
Email: mihir.kulkarni17@vit.edu  
Email: neeraj.kumbhojkar17@vit.edu  
\*Corresponding author

**Abstract:** With the world moving towards new sustainable sources of power for automobiles, electric powertrain systems are considered to be suitable. The study focuses on modelling and analysis of electric two-wheelers and designing and analysis of planetary gear box. Based on the analysis and market survey, recommendations for primary components are given. The electric vehicle is analysed using the drive cycle data and modelled using vehicle dynamics equations (Transportation Secure Data Centre). The result of this analysis is the current profile requirement to be fulfilled by the battery pack. The battery modelling and analysis is done based on the equivalent circuit modelling (Jackey et al., 2013; Jackey et al., 2009). The current profiles and battery testing data are used as input to the battery model (Jackey et al., 2009; Hu et al., 2014; Decibels Labs Pvt. Ltd.). SOC and voltage variations were determined from this modelling. The transmission gear ratio and geometry was determined (TM4 Electrodynamics). The dynamic analysis and life cycle estimation of the gear box was done in Ricardo SABR (Ricardo Software, 2020).

**Keywords:** electric vehicle; planetary gear box; powertrain; battery; modelling.

**Reference** to this paper should be made as follows: Paranjape, A., Kulkarni, A., Kulkarni, M. and Kumbhojkar, N. (2023) 'Modelling and analysis of electric two-wheeler with novel planetary gear box transmission', *Int. J. Electric and Hybrid Vehicles*, Vol. 15, No. 1, pp.67–106.

**Biographical notes:** Aditya Paranjape completed his Mechanical Engineering from Vishwakarma Institute of Technology, Pune in 2021. He is currently working in TE Connectivity as a Product Development Engineer. He has completed internship at Automotive Research Association of India, in the domain of electric vehicles. His research interests include novel mobility solutions, designing and simulations

Amey Kulkarni is a Mechanical Engineering graduate from Vishwakarma Institute of Technology, Pune. He has pursued his internship at Engineering Design and SIMULATION (EDS) Department at the Automotive Research Association of India, Pune. He is currently working in electric two wheeler start-up named Simple Energy, Pvt., Ltd. in Bangalore, India.

Mihir Kulkarni is a graduate in Mechanical Engineering from Vishwakarma Institute of Technology at Pune. He was a part of SAE BAJA team as a Powertrain Department Head where his team achieved awards in multiple events. His research interest is automotive design and development.

Neeraj Kumbhojkar has completed his BTech from VIT, Pune. He has worked in automotive domain as a team member of SAE BAJA and intern in the field of powertrain design, during his bachelor's. He is working as a Product Development Engineer in Electrical Domain at Eaton India Innovation Centre, Pune. In this role, he has worked on design, analysis, modifications and testing of devices such as relays and circuit breakers. His research interests include contact system design for relays, modelling and simulation of electro-mechanical devices and systems.

---

## 1 Introduction

In India the number of mopeds/scooters owned is vastly greater than the number of cars. Now that the world is shifting towards electric vehicles and considerable progress has been made in four wheelers whereas there is a lack in development of electric scooters. As the average Indian gets more use out of scooter rather than a car it seems only logical that we take a solid next step in development of electric scooters which is long overdue (*Economic Times of India*, 2021).

A traditional electric scooter has its prime mover, i.e., electric motor mounted away from the wheel hub and then connected via a belt drive or a chain sprocket mechanism to the rear wheel. This arrangement has a few disadvantages such as high centre of gravity, frictional and slip losses in the belt drives and thus lower mechanical efficiency. The project shifts the position of the BLDC mid-drive motor to the rear wheel eliminating the need of any belt or chain drives reducing the frictional losses. Instead, a planetary gear box coupled to the hub motor for additional gear reduction and torque multiplication makes the transmission into a positive drive eliminating slip. This enhances the mechanical efficiency with the added benefit of higher sprung to un-sprung mass ratio giving benefit to the suspension (Cheng, 2009).

The project starts with basic analysis of the driving conditions, i.e., the drive cycle analysis of which gives the various forces acting on the scooter to help in the resistive force modelling and torque and rpm charts (Transportation Secure Data Centre). Motor selection was then done on the basis of nominal and peak wheel torque requirements considering the motor efficiency ranges at different torque vs. rpm values (Adegbohun et al., 2021). The need additional torque enhancement required was then bridged by the planetary gearbox. Final drive ratio based on the finalised motor specifications was then cross checked so as to keep the torque and rpm within the motor limits. Design and modelling of gearbox, battery and cell was then done simultaneously using various software such as Matlab, Simulink and SABR (Koniak and Czerepicki, 2017; White et al., 2019; Ricardo Software, 2020; Mathworks; Mathworks).

The uniqueness of the following study is that the electric powertrain of the moped consists of BLDC mid-drive motor coupled with planetary gearbox for speed reduction (Xue et al., 2008; Kwon et al., 2020). The advantage of using mid-drive motor in conjunction with planetary gear box is that co-axial transmission of power takes place

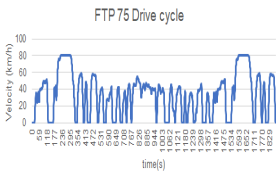
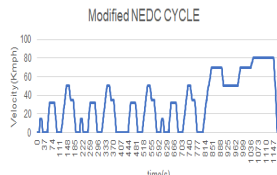
from motor to the gearbox and ultimately to the wheel which saves a lot of space. The method is suitable in this case as we require to replace the engine and belt-drive with electric powertrain (Gemmotors, 2021).

Thus, the project can be broadly divided into three major sections namely modelling and analysis of powertrain, design of planetary gearbox and cell modelling.

## 2 Powertrain modelling

The powertrain modelling is crucial for understanding the demands of the vehicle from the power producing devices in order to propel in a required fashion. The powertrain model takes the input of the driving patterns through the standardised drive cycles like FTP-75, WLTP, MNEDC (Transportation Secure Data Centre). This velocity vs. time data is crucial for building a basic powertrain model, which can be considered as a primitive step for further testing and development of the vehicle.

**Table 1** Characteristics of drive cycles (see online version for colours)

FTP 75	MNEDC	WLTP
Drive-cycle distance – 17.50km	Drive-cycle distance – 10.274km	Drive-cycle distance – 14.664km
		

**Table 2** Vehicle specifications

Coefficient of rolling resistance	0.015
Mass of vehicle(approximate) in kg	120
Mass of driver(average) in kg	80
Velocity	From drive cycle data
Frontal area of moped in $m^2$	0.877
Drag coefficient	0.22
Radius of wheel in m	0.127

### 2.1 Resistive forces

Any vehicle moving on the roads experiences four major types of resistances (Adegbohun et al., 2021). The vehicle can only propel forward when these resistive forces are overcome. The resistive forces are as follows:

- 1 Rolling resistance force (RRF) – This is a resistive force, and yet the most important force without which the vehicle cannot propel in any direction. This is the force due to friction. In case of an automobile, the wheels take the entire weight of the automobile as well as its passengers. The tyre and the road are in contact with each

other which gives rise to the friction. This friction force is in the opposite direction of the motion of the vehicle and hence is termed as a resistive force.

The RRF is dependent on various on-board factors like tyre compound, tyre pressure, vehicle speed. The tyre manufacturers have rigorously formulated the tyre compounds for optimum friction for safe, efficient and comfortable driving. The tyre pressure is prescribed for better driving experience. The following graph shows the relation between coefficient of friction and velocity for different tyre pressures. The research literature considers the standard value of 0.015 as the coefficient of friction for city driving (Xue et al., 2008; Adegbohun et al., 2021; Decibels Labs Pvt. Ltd.).

**Figure 1** Resistive force acting on a vehicle (see online version for colours)

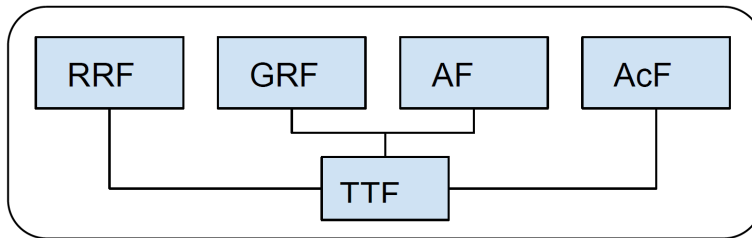
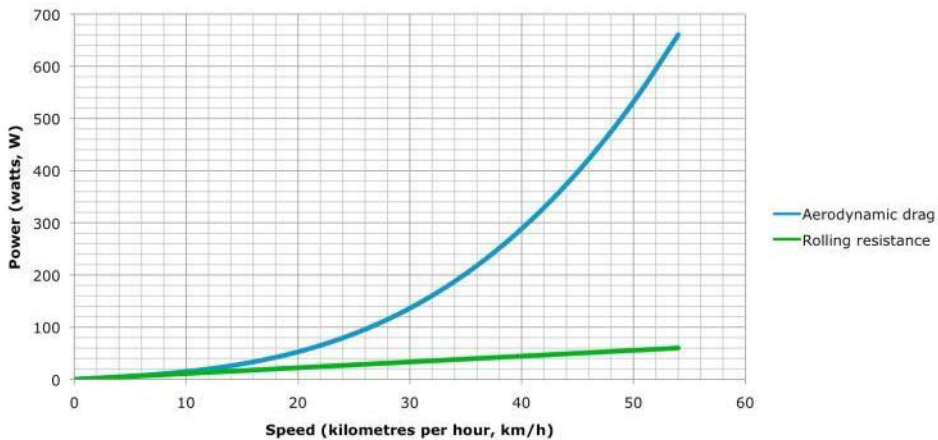


**Figure 2** Variation of (a) co-efficient of friction and (b) vehicle velocity for different tyre pressures (see online version for colours)



- 2 Grade resistance force (GRF) – The force, due to gravity, that resists the movement of a vehicle up a slope. The exact value of grade resistance may be found by multiplying the vehicle’s weight by the sine of the angle that the road surface makes with the horizontal. In case of our analysis, we have considered it to be zero for initial calculations.
- 3 Aerodynamic resistive force (AF) – The component of force exerted by the air on a solid object that is parallel and opposite to the direction of flow relative to the object. The aerodynamic force is a function of square of the velocity of the vehicle. Hence as the velocity of a vehicle increases the aerodynamic force increases exponentially.

**Figure 3** Variation of aerodynamic drag and rolling resistance with vehicle speed (see online version for colours)



- 4 Acceleration force ( $AcF$ ) – This is the force required to be generated in order to propel the vehicle at a required speed in a given amount of time. This resistive force is calculated by multiplying the gross vehicle mass and the acceleration. The acceleration is obtained by differentiating the velocity (obtained from drive cycle data) with respect to time.

Sum of these four resistive forces gives us the total tractive effort required by the vehicle in order to move as per the requirements. The total tractive force ( $TTF$ ) is given by,

$$TTF = RRF + GRF + AF + AcF$$

The TTF serves the base of all the further calculations and for modelling of the electric powertrain. The tractive force when multiplied by the radius of the wheel ( $R_w$ ) gives us the total wheel torque required to be generated to move the vehicle according to the drive cycle profile.

$$\text{Wheel torque}(T_w) = TTF \times R_x$$

Hence, the MATLAB simulink model gives two basic dynamic characteristics of the vehicle which are vehicle speed and vehicle wheel torque (Mathworks; Mathworks). These two parameters when multiplied give us the value of required power which is essential in selection of motor.

## 2.2 Motor selection

General types of motors used for electric vehicles are DC brushed motors, BLDC motors, induction motors, synchronous motors and switched reluctance motors (Xue et al., 2008).

In case of electric vehicles, brushless DC motors are used. The reasons include high efficiency and reliability. In our case we decided to consider an in-hub motor over traditional brushless DC motors due to factors such as, compactness and less bulky transmission systems.

**Table 3** The graphs show peak and nominal values of drive cycles (see online version for colours)

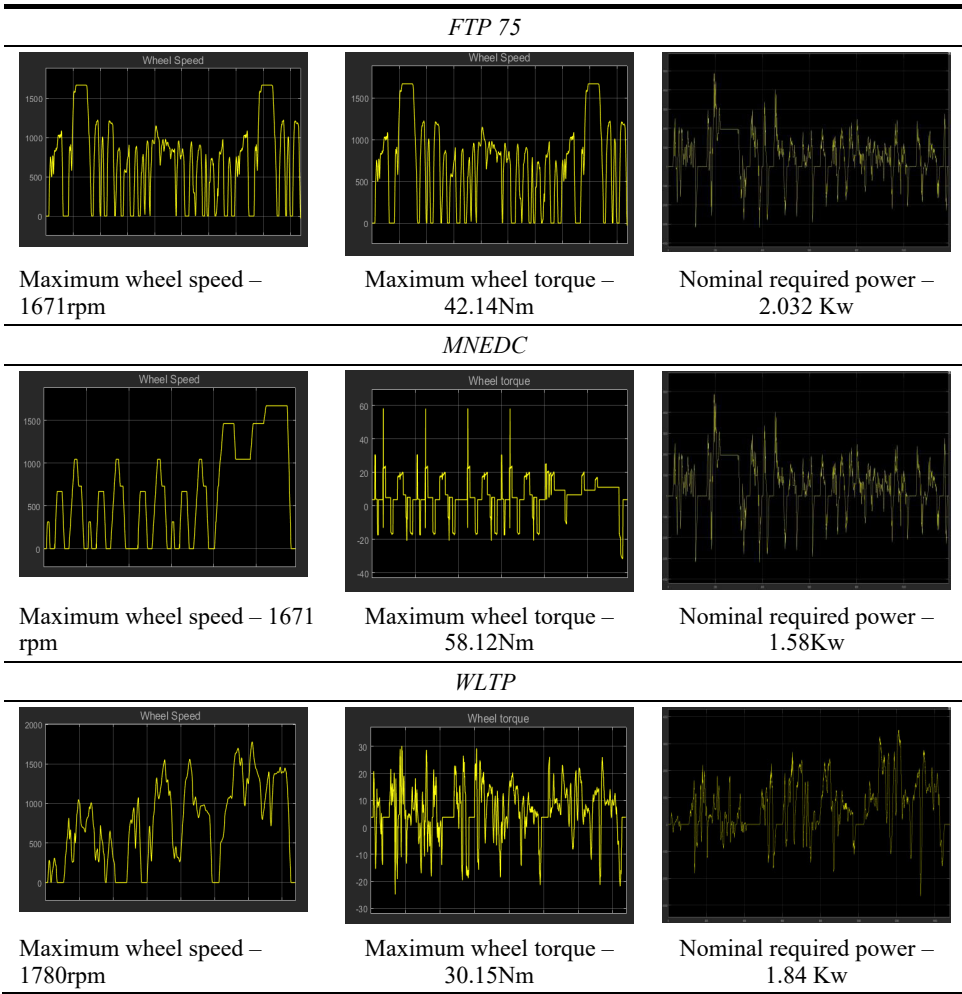
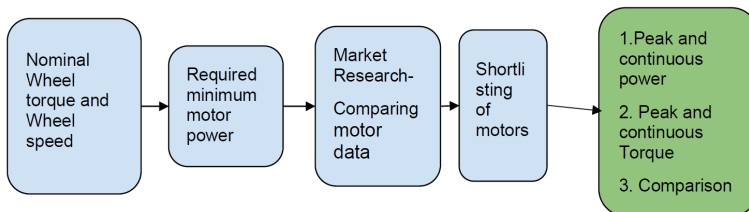


**Figure 4** Motor selection process flow (see online version for colours)



The nominal wheel torque, wheel speed and eventually minimum required power were obtained as shown in the previous study. From these parameters, market research was completed to find the best possible motor. The following Excel sheet shows the different hub motors from different manufacturers along with its specifications.

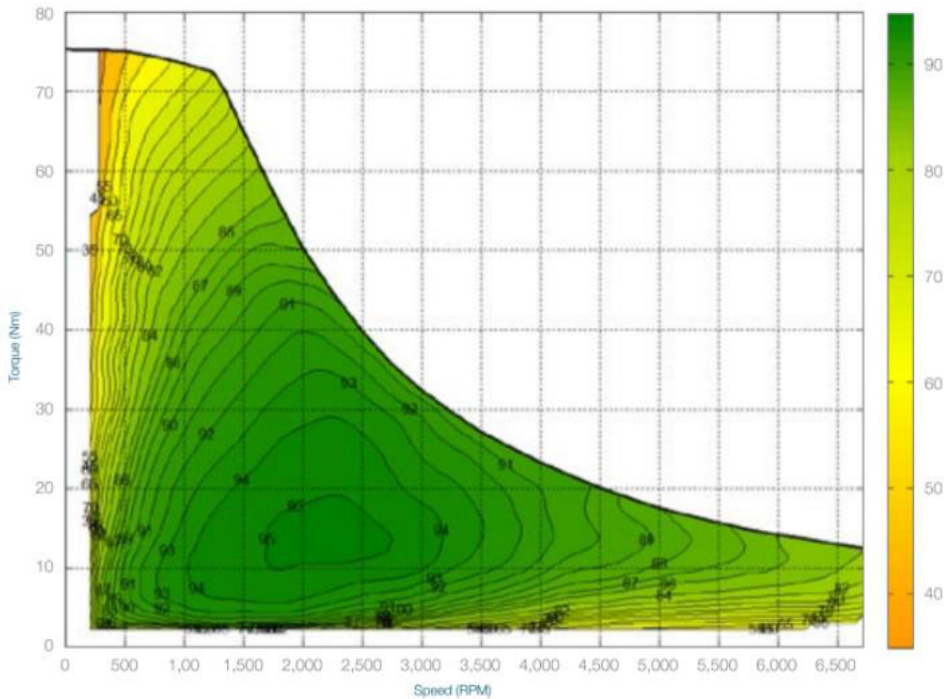
**Table 4** List of motor specifications of various motor manufacturers (see online version for colours)

Sr no.	Motor name	Power (peak)	Power (nominal)	Torque (peak)	Torque (nominal)	Speed	Cost	Weight	Current	Volts
1	Golden Motor	6 Kw	2-3 Kw	25 Nm	10 Nm	3,000-5,000		18 kg		
2	Golden Motor	10 Kw		29,230 Nm		2,000-6,000		17.7 kg	250 A	48 V
3	Miromax	7.5 Kw	3-5 Kw			2,000-6,000	770 Euro	15 kg		
4	QS Motor	--	5 Kw	240	-	20-70 Kmph	398\$	25 kg	80-150A	48 V
5	Luka EV	12.5								
6	Kelly controllers	11 KW	7 Kw	78 N-m	42 N-m	1,100-1,500 rpm	1,188 Euro		15-145	72 V
7	Kelly controllers	10 Kw	6 Kw	70 Nm	33 Nm	1,200-1,700 rpm	699 euro		12-125	72 V
8	Kelly controllers	10 Kw	6 Kw	70 Nm	33 Nm	1,200-1,700 rpm	933 euro		12-125	72 V
9	Motor series nova 15	4.2 Kw	-	1,724 Nm	-	2,353 rpm		2.5 kg	4.1 A	45 V
10	Motor series nova 15	5.8 Kw		1,795 Nm	-	3,120 rpm		2.5 kg	4.5 A	60 V
11	Motor series nova 15	8 Kw		3,038 Nm	-	2,519 rpm		2.5 kg	4.5 A	60 V
12	Motor series nova 15	11.6 Kw		3,107 Nm	-	5,369.3		2.5 kg	5.1 A	80 V
13	Motor series nova 15	12.7 Kw		3,056 Mcm	-	3,984 rpm		2.5kg	5.4 A	90 V
14	IPM 200-33	5-15 Kw	3-8 Kw	45 Nm	-	7,000 rpm		12 kg		24-96 V
15	IPM 200-50	7-20 Kw	3-10 Kw	75 Nm	-	7,000 rpm		15 kg		24-96 V
16	IPM-200-66	10-35 Kw	7-18 Kw	95 Nm	-	7,000 rpm		18 kg		24-96 V
17	Motor series nova 30	12.3 Kw	-	4,447 Nm	-	2,653 rpm				70 V
18	Motor series nova 30	14.3 Kw	-	4,478 Nm	-	3,056 rpm		6.5 kg		80 V
19	Motor series nova 30	16.4 Kw	-	4,552 Nm	-	3,456 rpm		6.5 kg		90 V
20	Motor series nova 30	18.2 Kw	-	4,506 Nm	-	3,855 rpm		6.5 kg		100 V
21	Motor series nova 30	20.4 Kw	-	4,587 Nm	-	4,250 rpm		6.5 kg		110 V
22	Motor series nova 30	22.6 Kw	-	4,590 Nm	-	4,722 rpm		6.5 kg		120 V

From the previous analysis, the nominal required power to propel the vehicle was considered as 2.98 kW. Similarly, the nominal torque value was considered while shortlisting the motor. This is important to have a compact transmission system with minimum gear ratio. Also, the motor voltage plays an important role in finalising the total number of cells in the battery pack.

Two motors were shortlisted for further analysis and comparison (TM4 ElectroDynamics). The further analysis is based on the efficiency of the motor at its rpm range for the given torque. It was done using the data provided by the manufacturer (TM4 ElectroDynamics).

**Figure 5** Efficiency map of shortlisted Motor as a function of motor speed and torque (see online version for colours)



The efficiency decreases as torque goes on increasing at a certain rpm. Also, the data suggest that as the rpm of the motor goes on increasing the torque it can deliver goes on decreasing. Here the transmission ratio can be selected from two approaches which are (Kwon et al., 2020),

- 1 Speed approach – By considering a nominal speed of motor where efficiency is maximum and hence calculating the transmission ratio. Here further validation is required about whether the obtained transmission ratio can satisfy the torque requirements at the wheel.
- 2 Torque approach – By considering the nominal torque of the motor at highest possible efficiency in a rpm range. The obtained transmission ratio is then used to

finalise the nominal rpm of the motor in the range of maximum efficiency for given value of torque.

In the selection, a torque approach was used for selecting the transmission ratio.

The study of the above graph shows that the maximum efficiency of the IPM 300 motor is concentrated in the rpm range of 1,500 to 2,500. Hence an optimum value of 5.10 Nm torque is considered. The nominal motor torque and nominal wheel torque was compared to get the transmission ratio. Going further, from the transmission ratio it is validated that whether the motor speed lies within the maximum efficiency zone.

Similarly, the transmission ratio is decided for IPM300 motor.

**Table 5** Motor parameter comparison

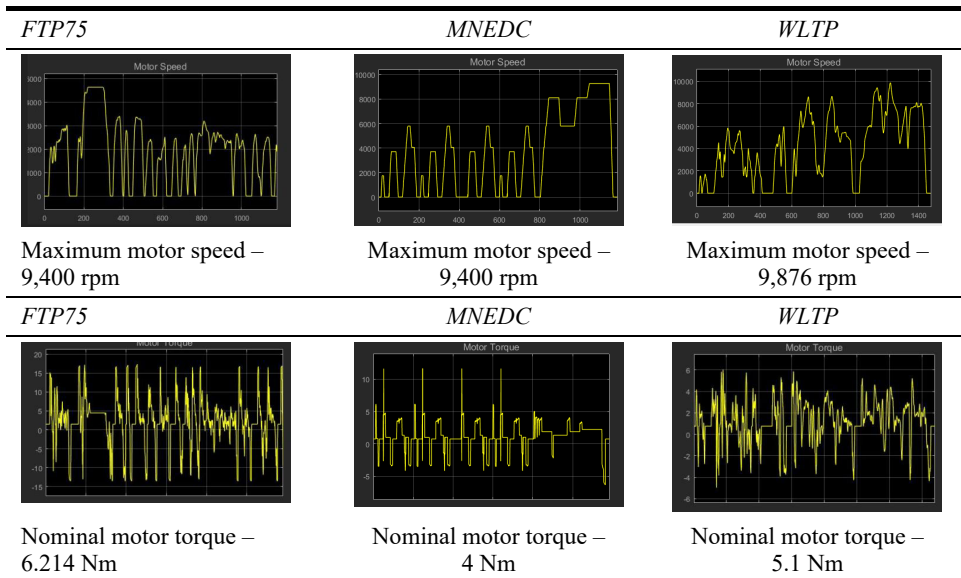
Nova 15	IPM 300
Nominal motor torque – 8.34Nm	Nominal motor torque – 5.10
Maximum motor speed – 9,400 rpm	Nominal motor speed – 9,600
Transmission ratio – 4	Transmission ratio – 5,625
Efficiency – 0.8	Efficiency – 0.9

The final motor selection was done on the basis of following points –

- 1 power to weight ratio
- 2 efficiency-torque-rpm relation
- 3 cost.

IPM 300 motor was finalised taking into consideration the above points. Table 6 shows the motor speed and torque curves for the selected motor

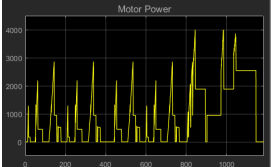
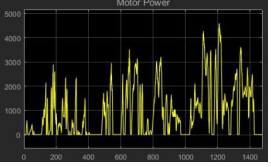
**Table 6** Motor speed curves for the selected motor (see online version for colours)



From the earlier study, the minimum required power in order to propel the vehicle according to the drive cycle characteristics was obtained. But there are several efficiencies like transmission efficiency and motor efficiency which need to be incorporated. Hence the final motor power required was obtained through the MATLAB Simulink model and was validated with the selected motor specifications (Ricardo Software, 2020; Mathworks).

The nominal power for all the drive cycles was greater than the required power and hence it can be concluded that the motor selection is validated.

**Table 7** Motor power curves (see online version for colours)

<i>FTP75</i>	<i>MNEDC</i>	<i>WLTP</i>
		
Nominal motor power – 4 KW	Nominal motor power – 2.832 Kw	Nominal motor power – 3 Kw

### 3 Planetary gearbox design

Planetary gearbox was selected as a torque multiplying unit due its highly compact nature and its high-speed reduction to space ratio which was one of the important goals of this project. The design parameters involved in design of the gearbox were

- 1 selection of number of teeth based on finalised gear ratio
- 2 dynamic design of shafts and gears based on detailed duty cycle
- 3 bearing life based on misalignment and load levels.

Dynamic design using ANSYS gave irregular and false results. This led to shift in software from ANSYS to a Ricardo software called SABR. This enhanced the design process and satisfied the objective of dynamic design for calculation of life of the components.

#### 3.1 Selection of no. of teeth

The suitable gear ratio for given vehicle application is 5.5 for Nova BLDC motor powered by Li-ion battery pack and tested for different drive cycles. The planetary gearbox assembly is most suitable gearbox in our application considering the space constraints. Planetary gears are able to transmit high levels of torque. The combination of compact size, large speed reduction and high torque transmission makes planetary gearboxes a suitable choice for our space-constrained application thus leading to co-axial motor shaft coupled to gearbox shaft and output shaft of gearbox coupled finally to the wheel.

**Table 8** Iterations on gear teeth based on finalised gear ratio (see online version for colours)

Gear ratio	Nominal motor RPM	Nominal wheel RPM	No. of teeth on gears										Corrected gear ratio	(Max motor torque) required	(Max motor RPM) required
			Zs	Zr	Zp	(Zs) corrected	(Zp) corrected	(Zr) corrected	(Zs) corrected	(Zp) corrected	(Zr) corrected	(Zr) corrected			
4	2,000	500	15	45	15	15	15	45	15	15	15	4	35	3,400	
4	2,000	500	16	48	16	16	48	16	16	16	16	4	35	3,400	
4	2,000	500	17	51	17	17	51	17	17	17	17	4	35	3,400	
5.55	2,000	360.3603604	16	72.8	28.4	16	74	29	29	29	29	5.625	24.888	4,781.250	
5.55	2,000	360.3603604	18	81.9	31.95	18	80	31	31	31	31	5.444	25.714	4,627.777	
5.55	2,000	360.3603604	19	86.45	33.725	19	87	34	34	34	34	5.578	25.094	4,742.105	
5.55	2,000	360.3603604	20	91	35.5	20	90	35	35	35	35	5.504	25.4325	4,678.508	
5.55	2,000	360.3603604	21	95.55	37.275	21	97	38	38	38	38	5.619	24.915	4,776.190	
5.55	2,000	360.3603604	22	100.1	39.05	22	100	39	39	39	39	5.545	25.245	4,713.636	
5.55	2,000	360.3603604	23	104.65	40.825	23	103	40	40	40	40	5.478	25.555	4,656.521	
5.55	2,000	360.3603604	24	109.2	42.6	24	110	43	43	43	43	5.583	25.074	4,745.833	

The planetary gearbox consists of ring gear, planet gear and sun gear and the planet carrier. For speed reductions, the sun gear is driving gear driven by the Nova motor. Ring gear in this case is stationary making the planet gear revolve around the sun gear as well as rotate. Planet gears are one or more than one. We have considered three planets for efficient load transfer. The carrier is attached at centre points of these planet gears and then coupled to output shaft thus providing the desired output speed reduction ratio.

The iterations were performed on Excel and the number of teeth was finalised considering space and strength criteria.

### 3.2 Gear design

Following is the list of acronyms used while discussing planetary gearbox further.

- $R_s$  and  $D_s$  = Radius and diameter of sun gear respectively,  $Z_s$  = Number of teeth on sun
- $R_p$  and  $D_p$  = Radius and diameter of planet gear respectively,  $Z_p$  = Number of teeth on planet gear
- $R_r$  and  $D_r$  = Radius and diameter of ring gear respectively,  $Z_r$  = Number of teeth on ring gear

Gear ratio for planetary gearbox system is given by

$$i = \frac{\text{Angular velocity of driving gear}}{\text{Angular velocity of planet-carrier}} = \frac{\text{Angular velocity of sun gear}(\omega_s)}{\text{Angular velocity of planet-carrier}(\omega_c)} \quad (1)$$

Pitch line velocity of the sun gear ( $V_s$ ) =  $\omega_s * R_s$ .

Pitch line velocity of the planet-carrier ( $V_c$ ) =  $\omega_c * R_p$ .

Pitch line velocity of the sun gear ( $V_s$ ) = 2 \* Pitch line velocity of the planet-carrier ( $V_c$ ),

$$i = \frac{2 * R_p + 2 * R_s}{2 * R_s} = \frac{R_r - R_s + 2 * R_s}{R_s}$$

Thus

$$i = \frac{R_s + R_r}{R_s} = 1 + \frac{R_r}{R_s} \quad (2)$$

The gear ratio formula for planetary gearbox with ring gear stationary also can be rewritten as

$$i = 1 + \frac{Z_r}{Z_s} \quad (3)$$

Let  $Z_p = 16$  for gear ratio 5.5 then by using (1) we get,  $Z_r = 72.8$  which is not a whole number. Thus, gear ratio needs to be corrected to get this a whole number.

If  $Z_r = 74$  and  $Z_s = 16$  the gear ratio is 5.625.

The final gear ratio selected thus is 5.625.

We also know the relation,

$$R_s + 2 * R_p = R_r \dots \quad (4)$$

Thus, as a result, we also get

$$Z_p = \frac{(Z_r - Z_s)}{2} \quad (5)$$

Therefore, for  $Z_r = 74$  and  $Z_s = 16$  we get  $Z_p = 29$ .

Helical gears are used in the above planetary gearbox arrangement for the following reasons:

- 1 The main reason for helical gears being used is the increased number of teeth in contact at any given time thus leading to greater contact ratio compared to spur gears.
- 2 For smoother and quieter operation.
- 3 Helical gears are generally used in high-speed applications. In our case, the motor speed can go as high as 6,000 rpm.

The normal module ( $m_n$ ) considered for the helical gears = 1.75 mm, helix angle ( $\Psi$ ) = 20 degrees, normal pressure angle ( $\alpha_n$ ) = 20 degrees. Sun gear has right-hand threads while planet and ring gear have left.

Pitch circle diameters of the corresponding gears can be determined by using relation

$$D = \frac{z * m}{\cos(\Psi)} \quad (6)$$

By considering empirical relation of facewidth of gears ( $b$ ) =  $10 * m$ ,  $b = 18$  mm in this case.

Material for the gears considered is AISI 9310. 9310 is the designation in both the SAE and AISI systems for this material. Among alloy steels, the composition of SAE-AISI 9310 steel is notable for including nickel (Ni) and containing a comparatively high amount of chromium (Cr). Ni is used to improve mechanical properties, and to make the alloy easier to heat treat. Cr is used to improve corrosion resistance and most mechanical properties (particularly at higher temperatures).

**Table 9** Material composition

<i>Material SAE 9310-chemical composition</i>	
Element	Composition (%)
Carbon (C)	0.008 to 0.013
Nickel (Ni)	3 to 3.5
Chromium (Cr)	1 to 1.4
Manganese (Mn)	0.45 to 0.65
Silicon	0.2 to 0.35

Material ultimate tensile strength ranges between 850–1,000 MPa and yield strength between 450–570 MPa and modulus of elasticity of 190 GPa. Carburised and heat treated it can develop hard wear resistant case of HRC (Rockwell C-scale) 54–57 or Rockwell Hardness of 592 BHN.

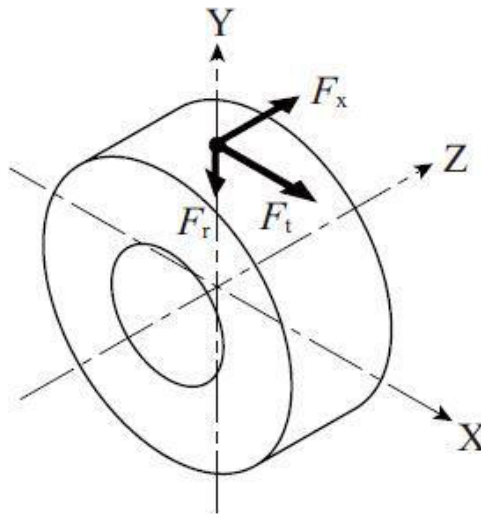
As shown in the Figure 6, three different forces act on helical gears in contact viz.

- a Tangential component ( $F_t$ ) – It acts along the X-axis as shown in above diagram. The direction of tangential force depends upon sense of rotation. For the driven gear it is always in the same direction and for the driving gear it is in opposite direction. Thus, when sun gear rotates in anti-clockwise direction,  $F_t$  acts along + X-axis on sun gear while -X-axis on planet-gear and thus acts on +X-axis on ring-gear.
- b Thrust component ( $F_a$ ) – It acts along the Z-axis as shown in the above diagram. It depends upon right/left hand of threads and sense of rotation. The sun gear which is driving gear has right hand threads and rotates in anti-clockwise sense thus thrust component acts along -Z-axis on sun while + Z-axis on planet gear.
- c Radial component ( $F_r$ ) – It always acts towards the centre of the gear. Thus along Y-axis for sun and planet gear.

**Table 10** Design analysis parameters

<i>Parameter</i>	<i>Value</i>
Tangential load ( $F_t$ )	1,006.7979 N
Dynamic load ( $F_d$ )	1,174.3123 N
Beam strength ( $S_b$ )	3,317.996 MPa
Wear strength ( $S_w$ )	2,421.21N
FOS (bending)	1.36
FOS (wear)	1.4621

**Figure 6** Helical gear force analysis



We check whether the design is safe for given loads.

The bending moment acting on sun-planet gear is given by

$$Mt = \frac{60 \cdot 10^6 \cdot P}{2 \cdot \pi \cdot N_s} \quad (7)$$

By using the above equation, we get  $Mt = 15,000 \text{ N-mm} = 15 \text{ N-m}$

$$F_t \frac{2 \cdot Mt}{D_s} = 1006.7969 \text{ N} \dots \quad (8)$$

$$F_a = F_t \cdot \tan(\psi) = 366.495 \text{ N} \dots \quad (9)$$

$$F_r = F_t \cdot \frac{\tan(\alpha_n)}{\cos(\psi_m)} = 390.023 \text{ N} \dots \quad (10)$$

Beam strength equation for helical gears is given by

$$S_b = m \cdot b \cdot \sigma \cdot Y \dots \quad (11)$$

Y is the Lewis form factor for virtual number of teeth  $(Z_s/\cos(\Psi))^3$ , i.e. 19.28

$Y = 0.316$ ,  $\sigma = (1000/3) = 333.33 \text{ MPa}$ ,  $m = 1.75$  and  $b = 18$

Thus,

$$S_b = 3317.996 \text{ MPa (bending strength)}$$

Pitch line velocity for sun gear is

$$v = \frac{\pi \cdot D_s \cdot N_s}{60 \times 10^3} \quad (12)$$

Thus,

$$v = 3.12 \text{ m / sec}$$

Tolerance for adjacent pitch error ( $e$ ) =  $6.701 \cdot 10^{-3} \text{ mm}$  (considering Grade 4 gear material)

$$\text{Deformation factor}(C) = 10,545 \text{ MPa}$$

Dynamic load is given by

$$F_d = \frac{21 \cdot v \cdot (c \cdot e \cdot b \cdot \cos^2(\psi) + F_t) \cdot \cos(\psi)}{21 \cdot v + \sqrt{(c \cdot e \cdot b \cdot \cos^2(\psi) + F_t)}} \quad (13)$$

$$F_d = 1174.3123 \text{ N}$$

$$\text{Effective load } (F_{eff}) = C_s \cdot F_t + F_d = 2432.808 \text{ N}$$

$$FOS(\text{bending}) = \frac{S_b}{5.6 + \sqrt{v}} = \frac{3317.996}{2432.808} = 1.36$$

$$\text{Velocity factor}(C_v) = \frac{5.6}{5.6 + \sqrt{v}} = 0.760$$

$$\text{Load - Stress factor}(K) = 0.16 \times (BHN/100)^2 = 5.607 \dots \quad (14)$$

$$\text{Ratio factor}(Q) = \frac{2 \times Z_p}{Z_p + Z_s} = 0.7111\dots \quad (15)$$

$$\text{Wear Strength}(S_w) = \frac{b \times Q \times D_s \times K}{\cos^2 \psi} 2421.21N$$

$$\text{Effectiveload acting on gear considering wear}(F_{eff}) = \frac{C_s}{C_v} \times Ft = 1655.9N$$

$$Fos(\text{wear}) = \frac{S_w}{F_{eff}} = 1.4621$$

Thus, design is safe considering beam strength and wear (Budynas, and Nisbett, 2011).

### 3.3 Dynamic design of gears and shafts

The geometry of shafts and gears were done in SABR software considering the strength, fatigue life of gears, shafts and bearings and also the ease of service and compactness of the gearbox. To decide the shaft dimensions first gear dimensions, need to be fixed based on strength and fatigue life calculations.

SABR offers a platform for gear design called GEAR in which variety of parameters are required as input on processing of which it gives output of bending stress, contact stress and fatigue life are obtained.

Basic parameters are module, number of teeth, helix angle, pressure angle and facewidth whose values for sun, planet and annulus gears were same.

Now as helical were opted in place of spur gears there is an important factor called Helical overlap ratio whose value needs to be greater than 1.1 so that we could have benefit is gained by having helical gears.

$$\text{Helical overlap ratio} = \frac{b * \sin(\alpha)}{Mn * \pi}$$

Considering above condition dimensions of gears were set as:

**Table 11** Geometric dimensions of gears

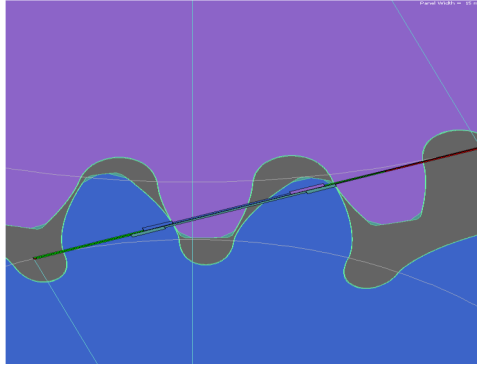
<i>Gear</i>	<i>Module</i>	<i>No. of teeth</i>	<i>Helix angle</i>
Sun gear	1.75	16	20
Planet gear	1.75	29	20
Annulus gear	1.75	74	20

Meshing criteria was another important parameter which decided backlash, interference and also contributes in prolonging life of the gear tooth. Inputs for these were min and max backlash, profile shift coefficient, outside diameter of gears, and target contact ratio. Iterations of these values gave a desired and optimum tooth profile.

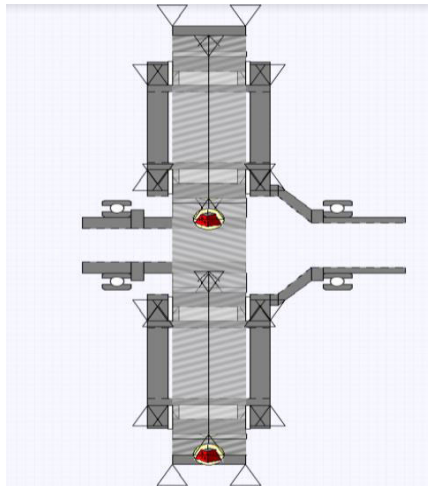
The gear profiles show path of contact and recess of both the meshing gears. Contact ratio is set to 1.75, max and min backlash values are 0.075mm and 0.050mm and profile shift coefficients of 0.779mm. This is preliminary stage of gear design in which basic dimensions of gears are set so that shaft geometry can be designed. Shaft design was then

further done considering the similar design and space parameters as discussed above. Bearings were added as supports and this led to finalisation of gearbox geometry.

**Figure 7** Gear tooth profile (see online version for colours)

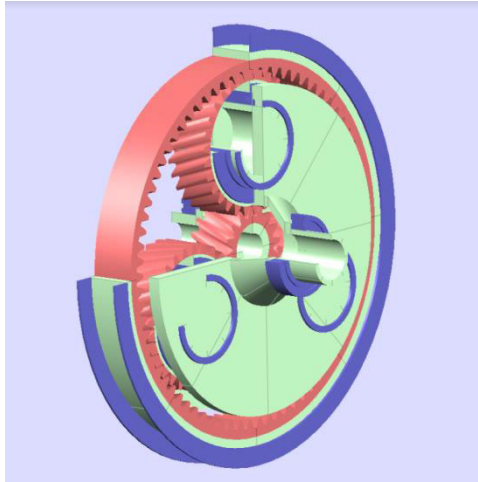


**Figure 8** 2D schematic of planetary gearbox (see online version for colours)



Next important step in design was the duty cycle to which the gears, shafts and bearing would be subjected. For this three standard drive cycles, i.e., FTP-75, WLTP, MNEDC were selected which resembled and covered maximum variety of driving conditions graphs of which are shown above.

From the graphs, vehicle data such as speed of vehicle and time were extracted. From the spec sheet of activa frontal area, tyre radius,  $C_d$  (Coefficient of drag) and literature survey giving values of rolling friction coefficient were obtained. These values gave time dependent values of motor torque and motor speed subsequently producing the required duty cycle. All the components inside the planetary gear box are subjected to this duty cycle.

**Figure 9** 3D model of planetary gearbox (see online version for colours)

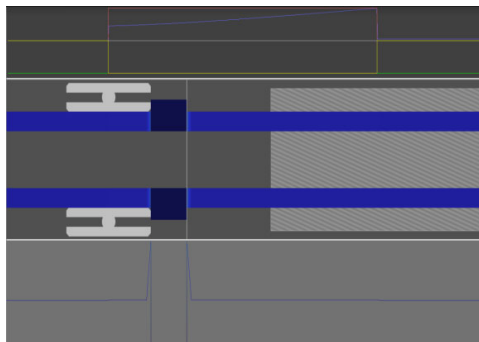
SABR then computes this duty cycle and gives us values of stress and deflections in shafts at various sections. The duty cycle as shown above was equally divided into sections from min value of torque (0 Nm) and maximum value of torque in normal running (16 Nm) are taken as first load case. For maximum acceleration the required torque value shoots up to 25 Nm. This accounts for second load case. Maximum stresses and deflections in normal driving occur at 16 Nm value and for accelerated drive at 25 Nm value. Following figures demonstrate these cases.

**Table 12** Shaft stress values at various load cases

<i>Load case/shaft</i>	<i>SUN-SHAFT</i>	<i>ANNULUS-SHAFT</i>	<i>CARRIER-SHAFT</i>	<i>*EPI* epi</i>
PF 1Nm	1 MPa	0 MPa	9 MPa	0 MPa
PF 2Nm	3 MPa	0 MPa	26 MPa	0 MPa
PF 3Nm	5 MPa	0 MPa	43 MPa	1 MPa
PF 4Nm	7 MPa	0 MPa	60 MPa	1 MPa
PF 5Nm	9 MPa	1 MPa	77 MPa	1 MPa
PF 6Nm	11 MPa	1 MPa	94 MPa	1 MPa
PF 7Nm	14 MPa	1 MPa	111 MPa	2 MPa
PF 8Nm	16 MPa	1 MPa	128 MPa	2 MPa
PF 9Nm	18 MPa	1 MPa	146 MPa	2 MPa
PF 10Nm	20 MPa	1 MPa	163 MPa	2 MPa
PF 11Nm	22 MPa	1 MPa	180 MPa	3 MPa
PF 12Nm	24 MPa	2 MPa	197 MPa	3 MPa
PF 13Nm	26 MPa	2 MPa	214 MPa	3 MPa
PF 14Nm	28 MPa	2 MPa	231 MPa	3 MPa
PF 15Nm	30 MPa	2 MPa	248 MPa	4 MPa
PF 16Nm	32 MPa	2 MPa	265 MPa	4 MPa
PF 25Nm	52 MPa	3 MPa	428 MPa	6 MPa

**Table 13** Epicyclic shaft stress values at various load cases

<i>Load case/shaft</i>	<i>discL</i>	<i>discR</i>	<i>pin1</i>	<i>p_body1</i>	<i>pin2</i>	<i>p_body2</i>	<i>pin3</i>	<i>p_body3</i>
PF 1Nm	0 MPa	0 MPa	0 MPa	0 MPa	0 MPa	0 MPa	0 MPa	0 MPa
PF 2Nm	0 MPa	0 MPa	0 MPa	0 MPa	0 MPa	0 MPa	0 MPa	0 MPa
PF 3Nm	0 MPa	0 MPa	1 MPa	0 MPa	1 MPa	0 MPa	1 MPa	0 MPa
PF 4Nm	0 MPa	0 MPa	1 MPa	0 MPa	1 MPa	0 MPa	1 MPa	0 MPa
PF 5Nm	0 MPa	0 MPa	1 MPa	0 MPa	1 MPa	0 MPa	1 MPa	0 MPa
PF 6Nm	0 MPa	0 MPa	1 MPa	0 MPa	1 MPa	0 MPa	1 MPa	0 MPa
PF 7Nm	0 MPa	0 MPa	2 MPa	0 MPa	2 MPa	0 MPa	2 MPa	0 MPa
PF 8Nm	0 MPa	0 MPa	2 MPa	0 MPa	2 MPa	0 MPa	2 MPa	0 MPa
PF 9Nm	0 MPa	0 MPa	2 MPa	0 MPa	2 MPa	0 MPa	2 MPa	0 MPa
PF 10Nm	0 MPa	0 MPa	2 MPa	0 MPa	2 MPa	0 MPa	2 MPa	0 MPa
PF 11Nm	0 MPa	0 MPa	3 MPa	0 MPa	3 MPa	0 MPa	3 MPa	0 MPa
PF 12Nm	0 MPa	0 MPa	3 MPa	0 MPa	3 MPa	0 MPa	3 MPa	0 MPa
PF 13Nm	0 MPa	0 MPa	3 MPa	0 MPa	3 MPa	0 MPa	3 MPa	0 MPa
PF 14Nm	0 MPa	0 MPa	3 MPa	0 MPa	3 MPa	0 MPa	3 MPa	0 MPa
PF 15Nm	0 MPa	0 MPa	4 MPa	0 MPa	4 MPa	0 MPa	4 MPa	0 MPa
PF 16Nm	0 MPa	0 MPa	4 MPa	0 MPa	4 MPa	0 MPa	4 MPa	0 MPa
PF 25Nm	0 MPa	0 MPa	6 MPa	0 MPa	6 MPa	0 MPa	6 MPa	0 MPa

**Figure 10** Sun shaft von-Misses stress for nominal torque (see online version for colours)

Figures 10 and 11 show a cross sectional view depicting the stress distribution of sun shaft for nominal and peak torques. The 3D CAD of the sun shaft is shown in Figures 12, 13 and 14 along with their respective displacements for nominal and maximum torque values as well.

Figures 15 and 16 show a cross sectional view depicting the stress distribution of carrier shaft for nominal and peak torques. The 3D CAD of the carrier shaft is shown in Figures 17, 18 and 19 along with their respective displacements for nominal and maximum torque values as well.

**Figure 11** Sun shaft von-mises stress for peak torque (see online version for colours)

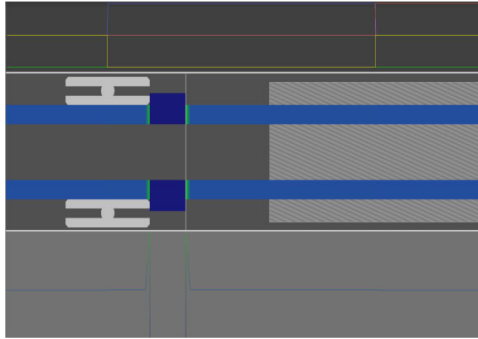


**Figure 12** Sun shaft (see online version for colours)

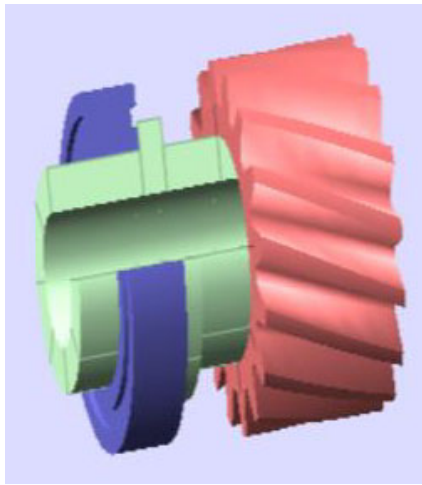


**Figure 13** Sun shaft displacement for nominal torque (see online version for colours)

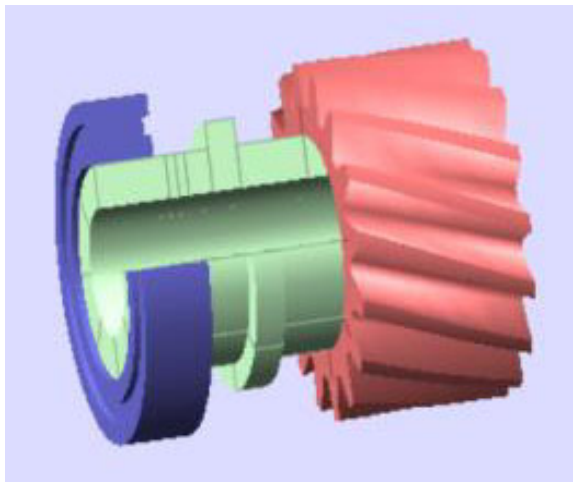


**Figure 14** Sun shaft displacement for peak torque (see online version for colours)

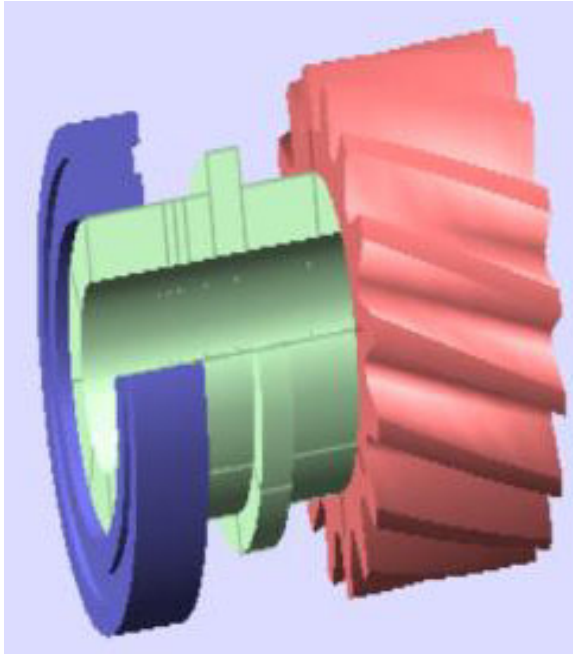
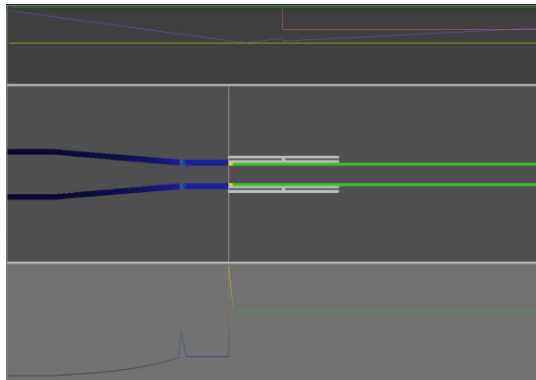


**Figure 15** Carrier shaft von-mises stress for nominal torque (see online version for colours)



Figures 20 and 21 show a cross sectional view depicting the stress distribution of planet shaft for nominal and peak torques. The 3D CAD of the planet shaft is shown in Figures 22, 23 and 24 along with their respective displacements for nominal and maximum torque values as well.

Figures 25 and 26 show a cross sectional view depicting the stress distribution of planet gear body shaft for nominal and peak torques. The 3D CAD of the planet gear body shaft is shown in Figures 27, 28 and 29 along with their respective displacements for nominal and maximum torque values as well.

**Figure 16** Carrier shaft von-mises stress for peak torque (see online version for colours)

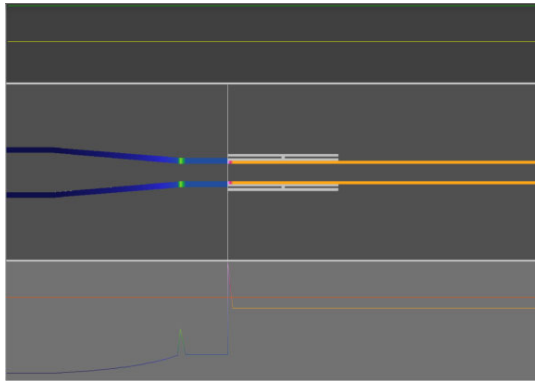


**Figure 17** Carrier shaft (see online version for colours)

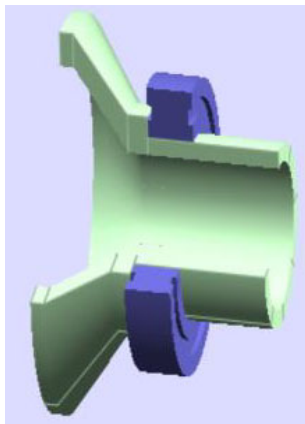


**Figure 18** Carrier shaft displacement for nominal torque (see online version for colours)

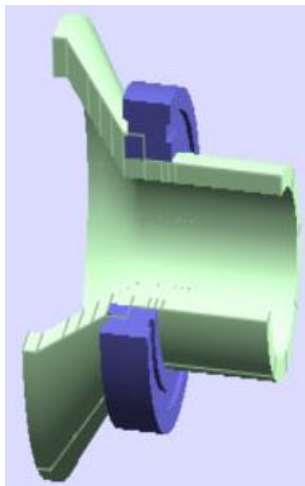


**Figure 19** Carrier shaft displacement for peak torque (see online version for colours)

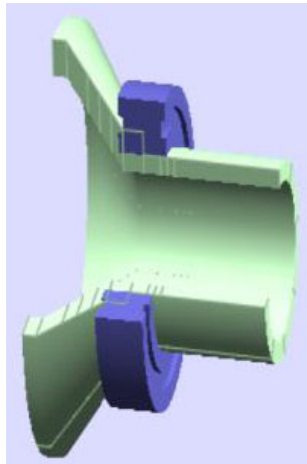


**Figure 20** Planet shaft von-mises for nominal torque (see online version for colours)

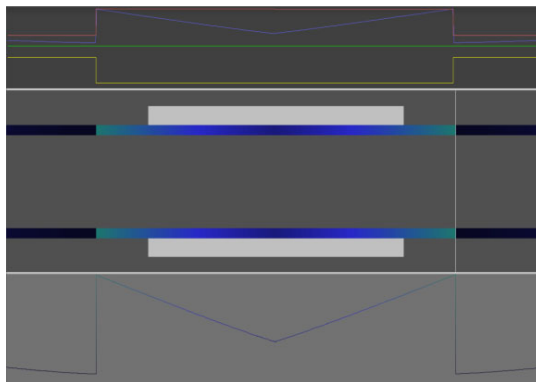


**Figure 21** Planet shaft von-mises stress for peak torque (see online version for colours)

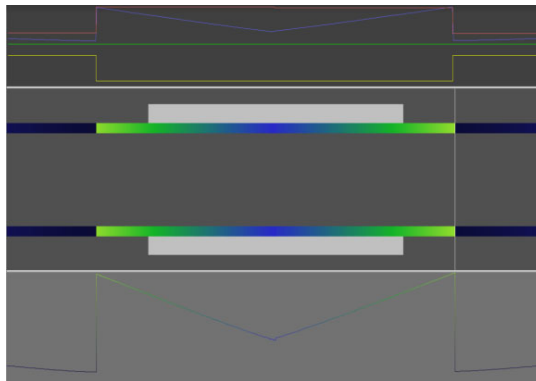


**Figure 22** Planet shaft (see online version for colours)

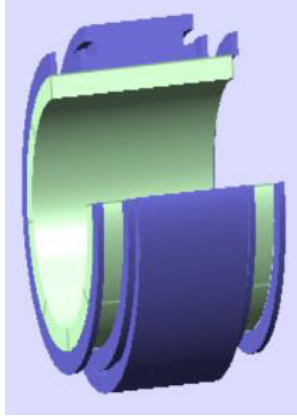


**Figure 23** Planet shaft displacement for nominal torque (see online version for colours)

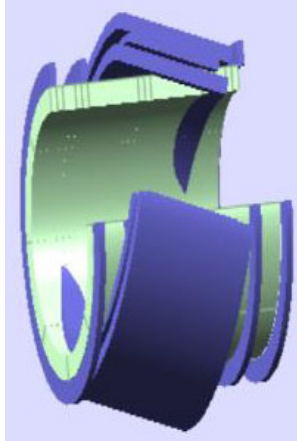


**Figure 24** Planet shaft displacement for peak torque (see online version for colours)

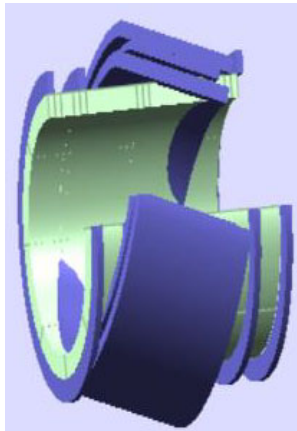


**Figure 25** Planet gear body von-mises stress for nominal torque (see online version for colours)

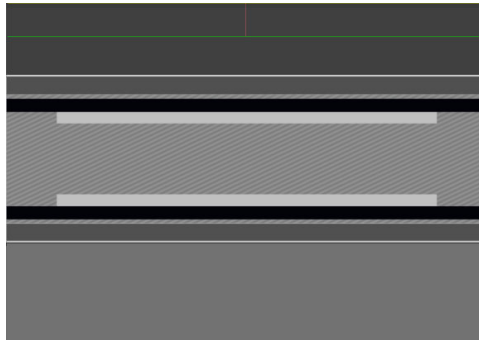


**Figure 26** Planet gear body von-mises stress for peak torque (see online version for colours)

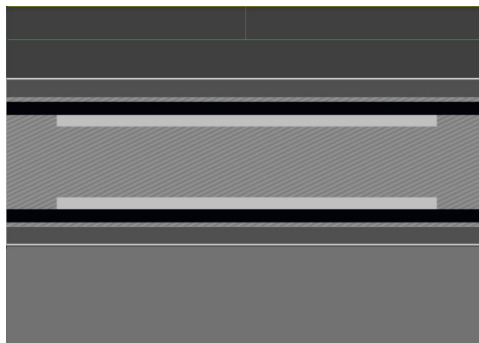


**Figure 27** Planet body (see online version for colours)

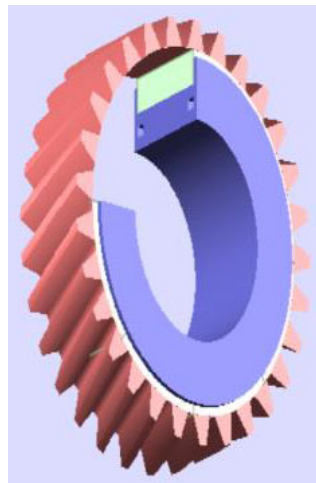
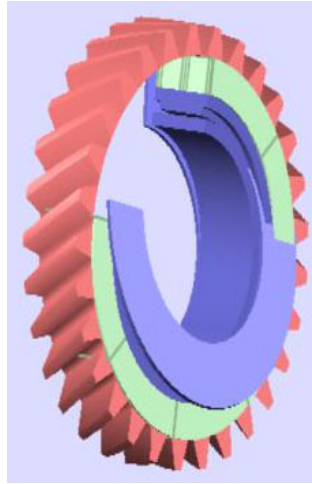


**Figure 28** Planet body displacement for nominal torque (see online version for colours)



Further design of the gears is done by optimising micro geometry of gears which includes optimising tip relief types of gear tooth and lead corrections which leads to even stress distribution for better contact stresses, transmission errors and local stiffnesses which are useful in NVH analysis of gears (White et al., 2019; Ricardo Software, 2020).

Figures 30 and 31 show stress distribution across sun-planet tooth facewidth for nominal and peak torque values respectively. Figures 32 and 33 show stress distribution across planet-annulus tooth facewidth for nominal and peak torque values respectively.

**Figure 29** Planet body displacement for peak torque (see online version for colours)

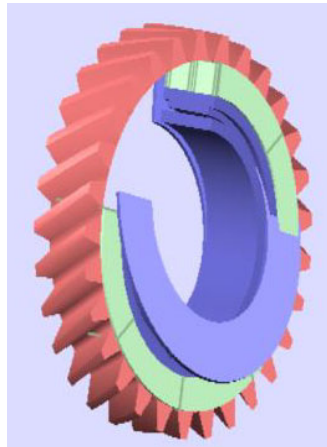


**Figure 30** Sun-planet tooth stress variation along facewidth for nominal torque (see online version for colours)

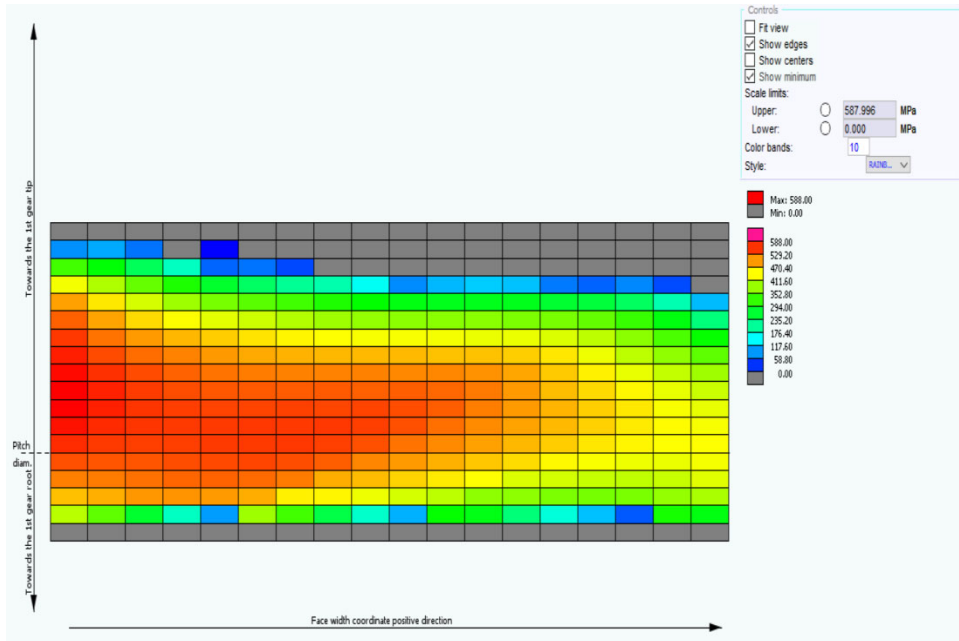


**Figure 31** Sun-planet tooth stress variation along facewidth for peak torque (see online version for colours)

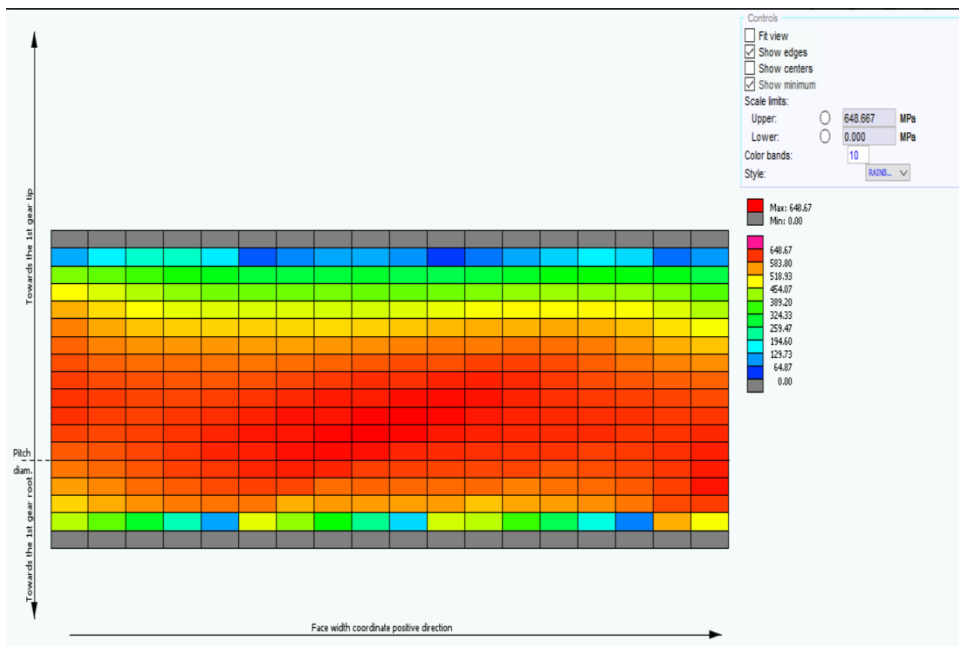


**Figure 32** Planet-annulus stress variation along facewidth for nominal torque (see online version for colours)

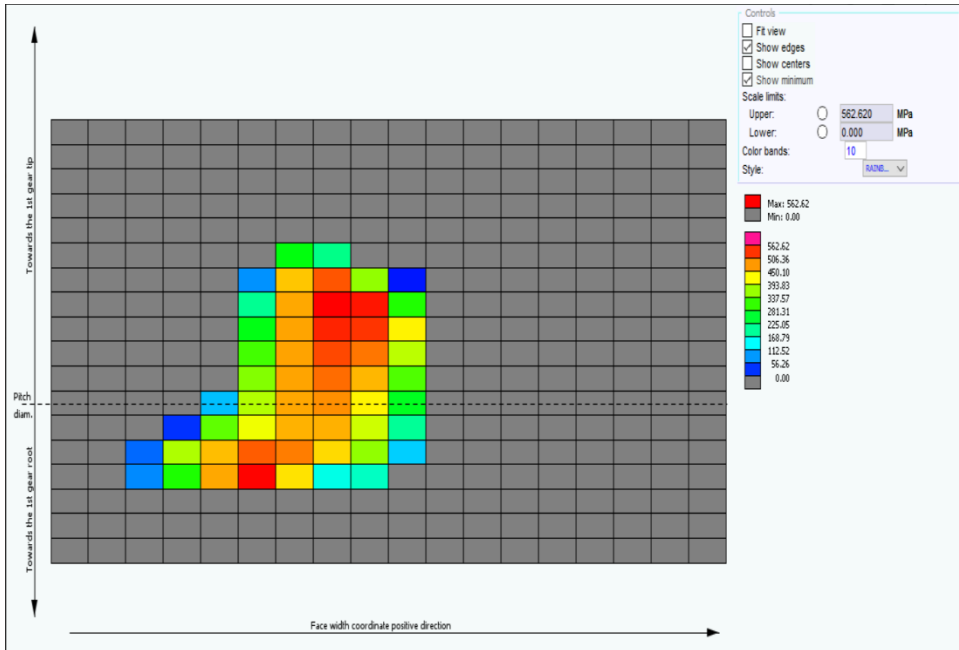


**Figure 33** Planet-annulus stress variation along facewidth for peak torque (see online version for colours)

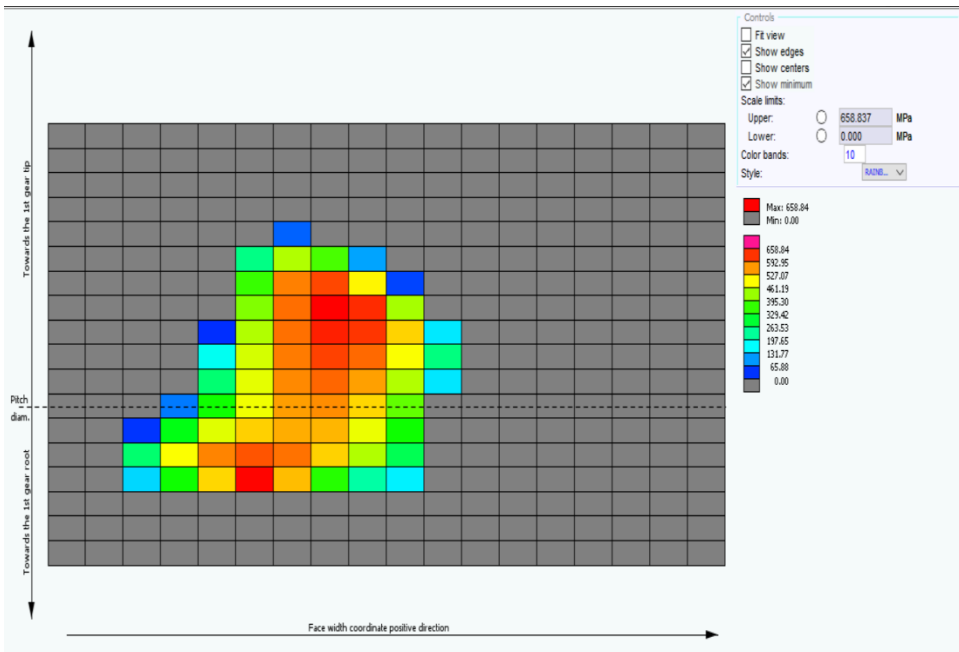


**Table 14** Fatigue life of sun and planet gears for 25Nm load case

<i>ISO 6336 Edition</i>			
<i>Property</i>	<i>Sun</i>	<i>Planet 1</i>	<i>Unit</i>
ISO Nom. Bending Stress $\sigma$ FO	58.715	53.505	Mpa
ISO Actual Bending Stress $\sigma$ F	190.609	173.697	Mpa
ISO Permissible Stress $\sigma$ FP	1,026.349	808.413	Mpa
ISO Bending Life	INFINITE	INFINITE	hour
ISO Bending Damage	0	0	%
ISO Safety Factor SF	5.385	4.654	
ISO Actual Contact Stress $\sigma$ H	1,080.091	1,080.091	Mpa
ISO Permissible Stress $\sigma$ HP	1,978.971	2,338.479	Mpa
ISO Contact life	INFINITE	INFINITE	hour
ISO Contact Damage	0	0	%
ISO Safety Factor SH	1.832	2.165	

As shown in Figures 30, 31, 32 and 33, stress values of various shafts is given for various load cases. To find the fatigue life of the shafts the given stress is plotted on the SN curve of the material selected i.e., SAE9310. In this case same material is used for gears and shafts. SABR doesn't give fatigue life, so for that we use SABR GEAR which considers the time for which a particular load case is applied in a drive cycle and then fatigue life is given relative to that service time (Ricardo Software, 2020). So for same material is we know the fatigue life for gear stresses we can find out shaft fatigue life as both are subjected to same duty cycles.

**Table 15** Fatigue life of annulus and planet gears for 25Nm load case

<i>ISO 6336 Edition</i>			
<i>Property</i>	<i>Annulus</i>	<i>Planet 1</i>	<i>Unit</i>
ISO Nom. Bending Stress $\sigma$ FO	47.758	46.03	Mpa
ISO Actual Bending Stress $\sigma$ F	196.692	206.907	Mpa
ISO Permissible Stress $\sigma$ FP	1,467.493	820.272	Mpa
ISO Bending Life	INFINITE	INFINITE	hour
ISO Bending Damage	0	0	%
ISO Safety Factor SF	7.461	3.964	
ISO Actual Contact Stress $\sigma$ H	609.137	509.137	Mpa
ISO Permissible Stress $\sigma$ HP	2,307.908	2,342.531	Mpa
ISO Contact life	INFINITE	INFINITE	hour
ISO Contact Damage	0	0	%
ISO Safety Factor SH	4.533	4.601	

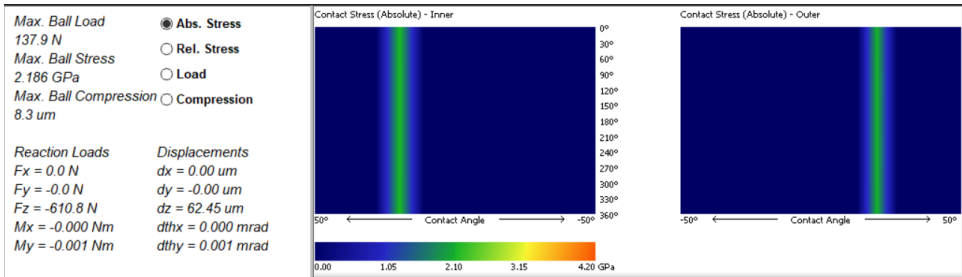
From Table 3, we can see that even for load case for accelerated drive which is the maximum stress condition we can see that stresses do not exceed 210 MPa and it leads to Infinite life. Now referring to Figure 9 and Table 12 there is not any load case for which

shaft stresses for any of the shaft exceed 210 MPa limit concluding that even shafts will have infinite life.

### 3.4 Bearing life calculations

Bearings are one of the most important components of any gearbox. Selection of bearing was a crucial decision as an under designed bearing would lead to catastrophic failure of every subsequent gearbox component and overdesigned bearing would unnecessarily increase weight of the assembly forcing to use expensive and more powerful prime movers inevitably increasing the cost of the vehicle.

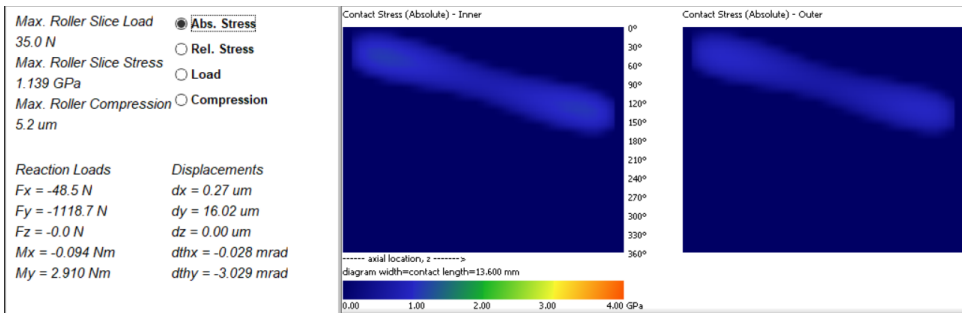
**Figure 34** Sun shaft bearing stress distribution (see online version for colours)



Helical gears add axial component of force which is to be supported by either tapered roller bearings or axial thrust bearings. But these are heavy and big bearings which would counter basic goal of the project.

Deep groove ball bearings were selected as the spherical balls do have some resistance against axial loads along with radial loads and are compact and small. Hence, proper selection of bearings which would sustain static loads and would at least have the design life (1,200 hrs).

**Figure 35** Planet shaft bearing stress distribution (see online version for colours)



The limit for maximum tilt in mrad according to standards is 3.8 mrad. The selected bearings have a very low (P/C) ratio so theoretically it has infinite life according to ISO 2007 which is the case for most of the bearings at lower loads and as seen in table the maximum stresses also do not cross the limiting value making the design safe.

**Figure 36** Carrier shaft bearing stress distribution (see online version for colours)

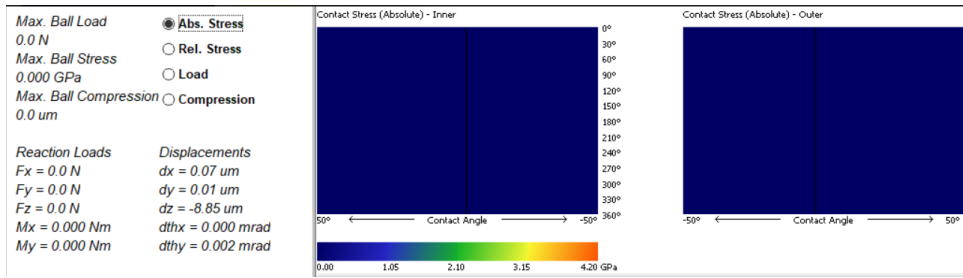


**Table 16** Bearing life, misalignment and stress data

Bearing	Type	Life (hrs)	Damage	Failure rate	Tilt(mrad)	Max. stress
Sun bearing	DG ball (SKF 61804)	68,133.9	1.7%	0 ppm	0.02	2,186
Carrier bearing	DG ball (SKF 61804)	Infinite	0%	0 ppm	0.06	0.056
Planet bearing	Needle roller	58564915.7	0%	0 ppm	3.03	1,139

**Figure 37** Assembly of planetary gearbox with motor and wheel



#### 4 Battery modelling

The motor power is the basis for the battery modelling. In an electric vehicle, the motor is controlled through the motor controller unit. This unit manages the current supply to the motor according to the driving conditions. The overall efficiency of the motor controller efficiency was considered as 0.85.

The battery power was converted into power per kilometre. This is done through the following equation.

$$Power\ per\ km = \int \left( \frac{Battery\ power}{D \times 3.6 \times 1000000} \right)$$

where  $D$  is the drive cycle distance.

Battery capacity in Wh/km is obtained by the following equation:

$$Battery\ capacity(Wh) = Power\ per\ km \times range$$

$$Battery\ capacity(Ah) = Battery\ capacity(Wh) / Voltage(V)$$

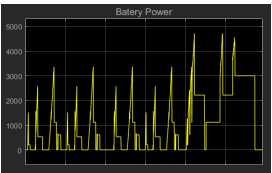
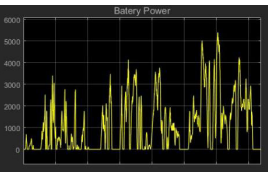
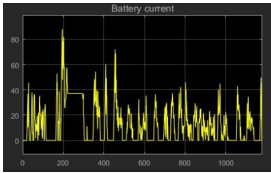
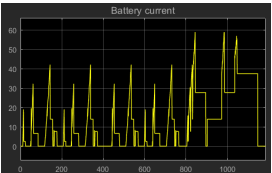
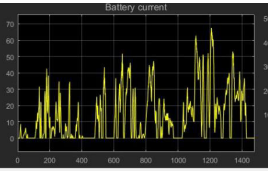
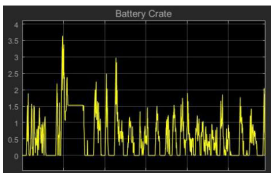
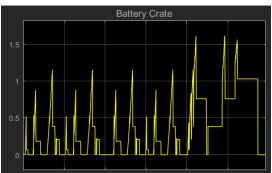
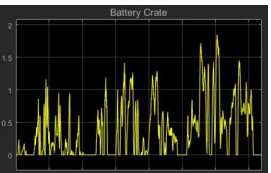
Further the battery current was calculated using the following equation:

$$Battery\ current = Battery\ power / Battery\ voltage$$

In the battery performance evaluation, C-rate plays a very important aspect.

By definition – the C-rate is a measure of the rate at which a battery is being discharged. It is defined as the discharge current divided by the theoretical current draw under which the battery would deliver its nominal rated capacity in one hour. A 1C discharge rate would deliver the battery’s rated capacity in 1 hour.

**Table 17** Battery power, current and C-rate curves (see online version for colours)

FTP 75	MNEDC	WLTP
		
Nominal battery power – 4,500 W	NOMINAL BATTERY POWER – 2,500 W	Nominal battery power – 2,800 W
		
Nominal battery current – 60 A	Nominal battery current – 35 A	Nominal battery current – 38 A
		
Nominal C-rate – 1.24	Nominal C-rate – 0.85	Nominal C-rate – 1.2

The C-rate is calculated using the following equation:

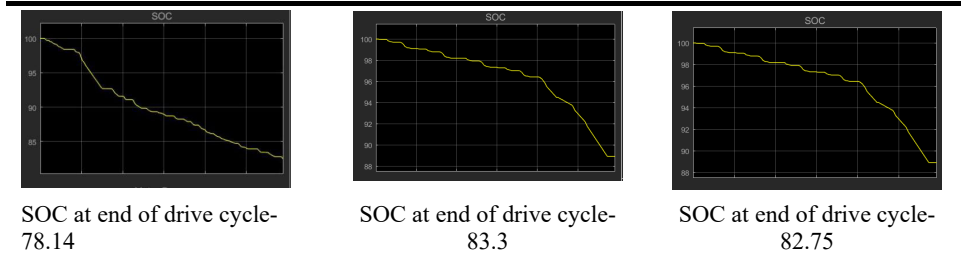
$$C\ -\ rate = Battery\ current / Battery\ capacity(Ah)$$

The state of charge (SOC) is defined as the ratio of the available capacity  $Q(t)$  and the maximum possible charge that can be stored in a battery. It is calculated by the following equation:

$$SOC = 100 \times \pm \int \frac{\text{Current}}{3600 \times C - \text{rate}} dt$$

Table 17 shows the curves for the battery power, battery current and C-Rate for the three drive cycles.

**Table 18** Variation of SOC over entire drive cycle range (see online version for colours)



## 5 Cell modelling

In this study equivalent circuit modelling (ECM) has been used to predict the behaviour of the battery under load conditions (Hu and Stanton, 2014). The use of mathematical models to predict the behaviour of the electrical system is called ECM (Jackey et al., 2009). In this the system is converted into an electrical circuit consisting of resistors, inductance and capacitors. Further this study shows the use of battery management system (BMS) to keep the battery functional under required limits of voltage current and temperature.

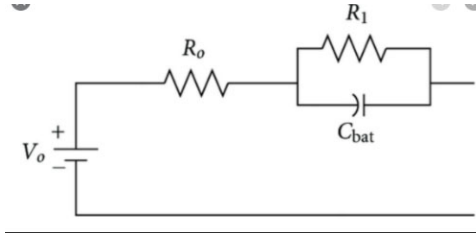
Lithium-ion batteries are used for the application, due to their high energy density and relatively long lifespan. To optimise the performance of a lithium-ion battery, it is essential to incorporate a BMS capable of monitoring specific data collected during battery charge and discharge. An effective BMS prevents battery overcharge and estimates remaining battery life so that the battery works efficiently and provides stable operating conditions. BMS data can also be used to accurately estimate the difference between the SOC and actual voltage and current conditions, which is necessary for certain aspects of a battery particular application, such as the precise estimation of the traveling distance of an electric vehicle, which is proportional to the life of its battery (Kumar et al., 2019).

From the powertrain simulations we have determined the motor torque and motor RPM required for the operation. The motor works on the current and potential difference provided by the battery, hence modelling of the battery is required to see whether the battery pack is capable of delivering the desired current under specified conditions. The simulations employ Thevenin equivalent circuit models consisting of a resistance, capacitance, and power source.

5.1 Thevenin's model

It is mainly composed of three parts, open-circuit voltage ( $U_{oc}$ ), internal resistances and RC pair. The internal resistances include the ohmic resistance  $R_o$ . The resistance and capacitance used parallel account for the non-linear ohmic and polarisation losses (Jackey et al., 2009). These are used to predict the non-linear response of the system. We have chosen Thevenin's model because the computational simplicity and the accuracy it gives satisfies the needs of project (Pei et al., 2018).

Figure 38 Thevenin's circuit



5.2 Cell selection

The Li-Ion battery in the vehicles is made of small cells which are connected in series and parallel. The battery pack capacity which was calculated from powertrain simulations and the voltage requirement of the battery was used to select the cell from the available cells in the market. The following cell was selected and the parameters were calculated from the cell spec sheet (Samsung Cell Data Sheet).

Table 19 Cell data (see online version for colours)

Samsung	ICR18650-25R		Cells in series	22.222	22
Nominal capacity	2,500	mAh	Cells in parallel	16	16
Minimum capacity	-	mAh	Total cells	352	
Charging voltage	4.2	V	Energy cell	9	Wh
Nominal voltage	3.6	V	Energy pack	3,168	Wh
Charging current(STD)	1,250	mA	Pack mass	15,840	G
	4,000	mA	Pack volume	7,413,120	mm <sup>3</sup>
Discharge current	500	mA	Gravimetric energy density	200	Wh/kg
	20,000	Ma	Volumetric energy density	427.35	Wh/L
Discharge cutoff voltage	2.5	V	Cost	52,800	Rs
Cell weight	45	G	Cost per KWh	16,666.667	Rs/KWh
Cell dimension(h*d)	65*18.40	mm2	C-rates-charge (nominal)	0.5	C
Operating temperature (Chg)	0 to 50	C	Discharge (nominal)	0.2	C
Operating temperature (DChg)	Minus 20 to 60	C			
Cost	150	Rupees			

**Figure 39** Voltage (SOC, temp) (see online version for colours)

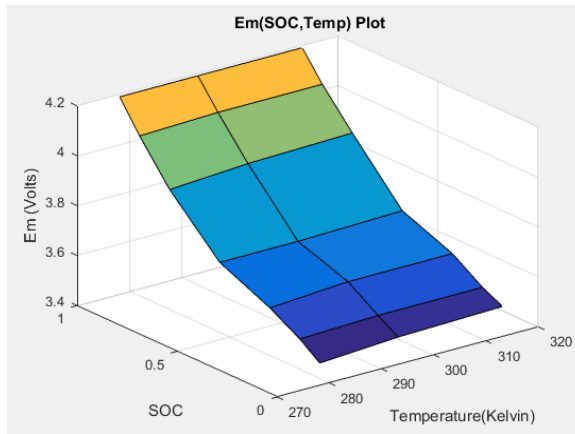


**Figure 40** Resistance (SOC, temp) (see online version for colours)

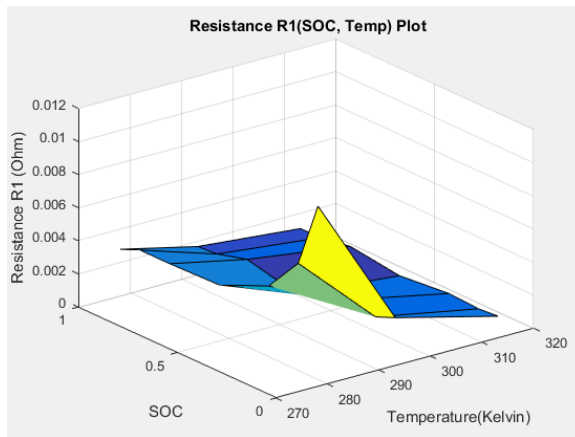


**Figure 41** Capacitance (SOC, temp) (see online version for colours)

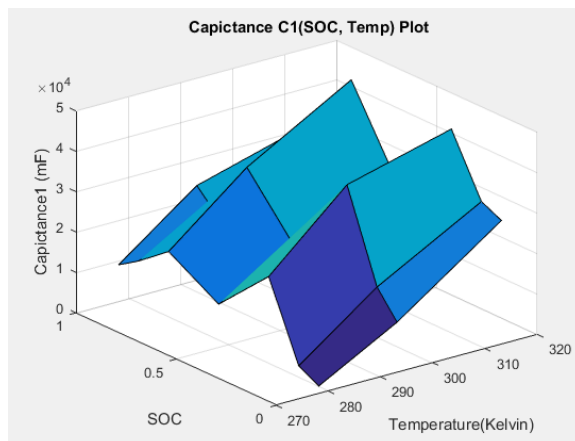
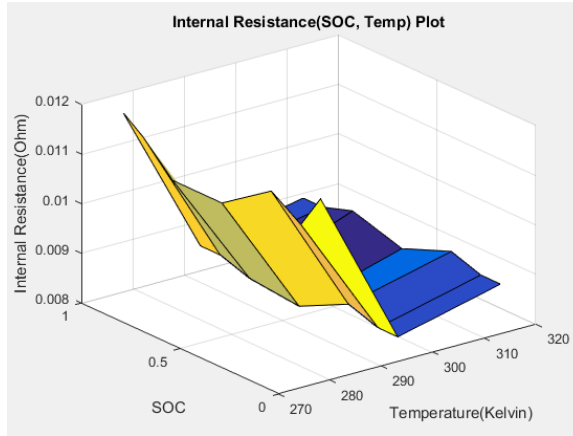


**Figure 42** Internal resistance (SOC, temp) (see online version for colours)



Cell data: For the study to predict how the model will behave under load conditions, cell testing data was recorded by a cell testing facility and was provided to us. The data includes the following

The cell was tested for three different temperatures and seven different SOC values, hence we get a total of 21 values of  $R_1$ ,  $R_0$ , open circuit voltage and  $C_{th}$  (How the cell testing is done is beyond the scope of this study). The 3D surface can be seen above. This data is essential for predicting the behaviour of the cell under the required drive cycle (i.e., the current profile).

**Table 20** Cell modelling results showing variation of current, temperature and terminal voltage

<i>FTP 75</i>	<i>MNEDC</i>	<i>WLTP</i>
Input current	Input current	Input current
Temperature	Temperature	Temperature
Terminal Voltage	Terminal Voltage	Terminal Voltage

### 5.3 Methodology for modelling

The current profiles that have been generated as result of the powertrain simulations are the major Input to the cell model. The modelling of the cell will gives variation of the crucial parameters of the cell such as, SOC, temperature, voltage and losses in the cell. This information is necessary for keeping the health of the battery in good condition (with help of a BMS) and monitoring performance of the battery. The following equations were used as for modelling the circuit of the battery.

$$\text{Energy} = \int \text{Power } dt = \int P \, dt \quad (16)$$

$$\text{Capacity of battery} = \int I \, dt \quad (17)$$

$$\text{State of charge (SOC)} = \text{Initial state of Charge (ISOC)} \pm \int \frac{I \, dt}{C * 3600} \quad (18)$$

$$\text{Power loss (P loss)} = I^2 \times R_o + I^2 \times R_{int} \quad (19)$$

$$\text{Temperature} = m \times C_p \times \Delta t = P_{loss} + hA\Delta t \quad (20)$$

$$m \times C_p \times \frac{d(T_{amb} - T)}{dt} = P_{loss} + hA\Delta t \quad (21)$$

$$\frac{d(T_{amb} - T)}{dt} = P_{loss} + \frac{h \times A}{m \times C_p} hA\Delta t \times (T_{amb} - T) \quad (22)$$

$$\int dT = \int \frac{P_{loss} - (h \times A \times (T_{amb} - T))}{m \times C_p} \quad (23)$$

The model is mainly divided into 3 sections

- 1 equivalent circuit model: – SOC and power losses are calculated
- 2 temperature estimation
- 3 terminal voltage estimation
- 4 results.

The crucial results of temperature, current and terminal voltage were derived from this study. The following are the results for three drive cycles

The results show the variation of temperature and terminal voltage with input current. In some of the cases above the voltage and temperature is rising above the specified limits mentioned by the cell manufacturer. Hence, we require a BMS.

## 6 Battery management system

Automotive BMS must be able to meet critical features such as voltage, temperature and current monitoring, battery SoC and cell balancing of lithium-ion (Li-ion) batteries (Plett,

2015). The BMS has the function to provide safety to the system during charging and discharging, hence BMS has to be modelled for both conditions.

Main functions are:

- 1 Battery protection in order to prevent operations outside its safe operating area.
- 2 Battery monitoring by estimating the battery pack SoC and state of health (SoH) during charging and discharging.
- 3 cell balancing and charge control.

### *6.1 BMS protection parameters*

- 1 Voltage: The voltage protection includes protection against over and under voltage. These circuits must be extremely responsive. Voltage can be measured using voltage divider circuit.
- 2 Current protection: Current can be measured using shunt resistor method or hall effect sensor. Overcurrent may occur due to:
  - a high demand from load
  - b cell with different C-rates
  - c an unbalanced battery packs
- 3 Temperature protection: NTC thermistor can be used. On a secondary level, thermal irreversible fuses can be used.

### *6.2 Cell balancing*

All the individual cells must have same individual SOC as far as possible during charging and discharging, The BMS avoids overcharging and undercharging.

### *6.3 Modelling of BMS*

The modelling of BMS is done using the logic gates. The values of temperature, current and voltage which are generated in the cell modelling are compared with limiting values given by the cell manufacturer. These values have to be compared during charging and discharging cases. In the study, when the system overshoots in a particular parameter, the system brings the parameter to set zero value. After each cycle the current profile is updated according to the BMS logic limits and is send back to the model as new current cycle. It works as a feedback mechanism.

## **7 Conclusions**

As discussed, due to lack of a substantial foundation in the field of EV in mopeds, upcoming manufacturers that wish to develop a custom EV powertrain suitable to their requirements, would now have a basis to do so using this study. The project describes in detail the motoring and regenerative curves of various parameters along with the torque and rpm data pertaining to the chosen drive cycle and it evidently will benefit the user in

multiple areas such as fatigue design of mechanical components by obtaining a duty cycle of stresses acting, predicting life and optimising the design, sizing the battery and motor. Mathematical modelling and simulation also inform the user about the expected behaviour and the zone in which the vehicle is operating for tuning the propulsion system, i.e., motor and battery to extract highest possible efficiency and in turn range of vehicle.

This work being in its infancy stage has its limitations as well as scope for improvement. The model described doesn't include the losses in electric components as accurately but gives a broader view of possible areas of losses.

In future in the fields of retro fitment, battery management and vehicle modelling, the work done in this project can prove useful as the user has all the data curves with them to efficiently tune the control systems of a battery for higher longevity and due to the sizing done will definitely impact retro fitment of EV mopeds.

## References

- Adegbohun, F., von Jouanne, A., Phillips, B., Agamloh, E. and Yokochi, A. (2021) 'High performance electric vehicle powertrain modeling, simulation and validation', *Energies*, Vol. 14, p.1493, <https://doi.org/10.3390/en14051493>.
- Budynas, R.G. and Nisbett, J.K. (2011) *Shigley's Mechanical Engineering Design*, 9th ed., McGraw Hill, USA, pp.733–765.
- Cheng, K.W.E. (2009) 'Recent development on electric vehicles', *International Conference on Power Electronics System and Applications*, Hong Kong, 20 May 2009 through 22 May 2009, Article number 5228598.
- Decibels Labs Pvt. Ltd. [online] <https://lms.decibelslab.com/> (accessed 12 June 2020).
- Economic Times of India* (2021) 'Why the future of electric vehicles in India looks bright', [online] <https://economictimes.indiatimes.com/industry/auto/auto-news/why-the-future-of-electric-vehicles-appears-bright-in-india/articleshow/81531959.cms?from=mdr> (accessed 1 June 2020).
- Gemmotors (2021) 'Gemmotors: in wheel motors and electric drive solutions', *Development of Electric Powertrain for Scooters – GEM Conversion|GEM Motors* [online] <https://www.gemmotors.si/> (accessed 19 June 2020).
- Hu, X. and Stanton, S. (2014) *A Complete Li-Ion Battery Simulation Model*, SAE Technical Paper 2014-01-1842, <https://doi.org/10.4271/2014-01-1842>.
- Jackey, R., Plett, G. and Klein, M. (2009) *Parameterization of a Battery Simulation Model Using Numerical Optimization Methods*, SAE Technical Paper 2009-01-1381, DOI:10.4271/2009-01-1381.
- Jackey, R., Saginaw, M., Sanghvi, P. and Gazzarri, J. (2013) *MathWorks, Battery Model Parameter Estimation Using a Layered Technique: an Example using a Lithium Iron Phosphate Cell*, SAE Technical paper 2013-01-1547, DOI:10.4271/2013-01-1547.
- Koniak, M. and Czerepicki, A. (2017) 'Selection of the battery pack parameters for an electric vehicle based on performance requirements', in *Materials Science and Engineering Conference Series*, Vol. 211, No. 1, p.12005, DOI:10.1088/1757-899X/211/1/012005.
- Kumar, R., Kaundinya, A., Shah, R., Ghugal, S. et al. (2019) *Design and Development of a Retrofit Solution for Converting a Conventional LCV into Parallel Hybrid Electric Vehicle*, SAE Technical Paper 2019-26-0117, <https://doi.org/10.4271/2019-26-0117>.
- Kwon, K., Seo, M. and Min, S. (2020) 'Multi-objective optimization of powertrain components for electric vehicles using a two-stage analysis model', *Int. J. Automot. Technol.*, Vol. 21, pp.1495–1505, <https://doi.org/10.1007/s12239-020-0141-5>.
- Mathworks [online] <https://in.mathworks.com/help/simulink/> (accessed 9 July 2020).

- Mathworks [online] <https://in.mathworks.com/products/simulink.html> (accessed 1 August 2020).
- Pei, Z., Zhao, X., Yuan, H., Peng, Z. and Wu, L. (2018) ‘An equivalent circuit model for lithium battery of electric vehicle considering self-healing characteristics’, <https://doi.org/10.1155/2018/5179758>.
- Plett, G.L. (2015) *Battery Management Systems*, Vol. 1, Artech House, USA, pp.75–130.
- Ricardo Software (2020) ‘SABR 2020.2 user’s manual’, [online] <https://software.ricardo.com/products/sabr> (accessed 29 August 2020).
- Samsung Cell Data Sheet [online] <https://robu.in/product/samsung-inr18650-25r-2500mah-li-ion-battery/> (accessed 24 September 2020).
- TM4 Electroynamics, *Dana TM4 – Electric and Hybrid E-Drive Systems* (accessed 15 September 2020).
- Transportation Secure Data Centre, *Transportation Secure Data Center | NREL* [online] (accessed 29 June 2020).
- White, G., Cunningham, G. and Doyle, D. (2019) *Design of an Electric Drive Transmission for a Formula Student Race Car*, SAE Technical Paper 2019-01-1295, <https://doi.org/10.4271/2019-01-1295>.
- Xue, X.D., Cheng, K.W.E. and Cheung, N.C. (2008) ‘Selection of electric motor drives for electric vehicles’, *2008 Australasian Universities Power Engineering Conference*, pp.1–6.